ACS OMEGA

http://pubs.acs.org/journal/acsodf

Article

Empowerment of Water-Evaporation-Induced Electric Generators via the Use of Metal Electrodes

Tina Tabrizizadeh, Zhe She, Kevin Stamplecoskie, and Guojun Liu*

Cite This: *ACS Omega* 2022, 7, 28275−28283

Read Online

ACCESS | Metrics & More | Article Recommendations | Supporting Information

ABSTRACT: As water rises in the pores of a partially immersed porous film due to capillary action, it carries along ions that are dissociated from the pore walls, generating a streaming current and potential. The water and current flows are sustained due to water evaporation from the unsubmerged surfaces. Traditionally, inert graphite (C) electrodes are used to construct water-evaporation-induced generators (WEIGs) that harness this electricity. WEIGs are environmentally friendly but have weak power outputs. Herein, we report on C/metal WEIGs that feature C top electrodes and metal bottom electrodes, as well as metal/metal WEIGs. Operating in a NaCl solution that facilitates the Galvanic corrosion of the metal (Cu, steel, and Al) electrodes, these Galvanic WEIGs outperform a C/C WEIG by thousands of times in power output. Equally interestingly, the asymmetric environments and potential differences between the two electrodes of a WEIG facilitate metal corrosion and fabrication of compact Galvanic WEIGs. This study clearly shows that one should choose electrodes with caution for the construction of true WEIGs.

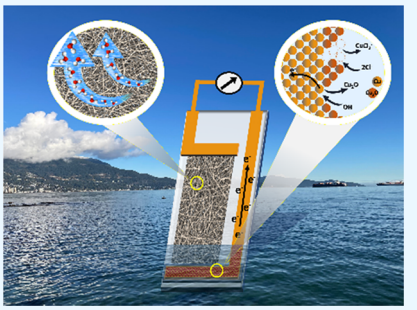

INTRODUCTION

As water flows in the channels of a porous medium, it carries along ions that have dissociated from functionalities such as phenol groups on the pore walls, generating a streaming current and potential.[1−5] A streaming current is also produced by water rise caused by capillary action in the hydrophilic pores of a partially immersed thin film, and this water and current flow are sustained due to water evaporation from the unsubmerged surfaces.[6] Since the seminal report of Guo and Zhou on the harnessing of this streaming current via a water-evaporation-induced generator (WEIG) fabricated using films of fused carbon soot particles,[6−8] WEIGs have also been constructed from carbon nanotube mats,[9] partially fused cellulose acetate nanofiber mats,[10] cotton fabric coated with carbon particles,[11,12] films of Al_2O_3 and other metal oxide particles,[13] porous printed graphene oxide films,[14] and 3D graphene membranes.[15,16] We have also recently reported on WEIGs from carbon nanofiber mats (CNMs),[17] carbon nanotube mats,[18] and thin-layer chromatography plates.[19] While WEIGs convert thermal energy from their surroundings into electricity and are environmentally friendly,[7] the areal power densities of these devices are typically below ∼100 nW/cm^2.[17] The low power densities limit their applicability.

To boost the power densities of WEIGs, Dao et al.[9] produced a floating WEIG from a carbon nanotube mat with two ends connected to one another via "protected" Zn wires. The high electric output of 17.4 μW/cm^2 was later determined to arise mostly from the corrosion of the Zn wires because the replacement of the Zn wires with inert Au wires drastically decreased the produced power.[20] Sun and co-workers[21,22] fabricated Si pillar arrays. Water rising in such parallel pillars with spacing in the nanometer range (smaller than the Debye length of the electric double layers surrounding these pillars) produced up to 10 μW/cm^2 of electricity. Herein, we report on the increase in the output of our CNM-based WEIGs from 0.083 to 29 μW/cm^2.

The harvesting or the need to determine accurately the magnitude of the streaming current has required the use of "inert" electrodes, including graphite (C) electrodes,[23] in the fabrication of WEIGs. Cu foils corrode in salty water but have still been used by accident or mistake as the electrodes.[9,14,17,24,25] Unfortunately, the contributions made by the corrosion of Cu to the output of WEIGs have not been properly acknowledged. We report here the purposeful use of corroding Cu, steel (St), or Al electrodes to construct Galvanic WEIGs. Here, the alloy steel rather than a pure metal is utilized because of its wide use and ubiquitous occurrence around us. We compare the short-circuit currents I_s and open-circuit voltages V_o of C/C (top/bottom electrode), C/metal, and metal/metal WEIGs obtained under different conditions to gauge the contributions made to these quantities by Galvanic chemistry. Operating in a 0.100 M NaCl solution, the I_sV_o values of metal/metal WEIGs may be 3 orders of magnitude higher than that of a C/C WEIG, suggesting the drastic power

Received: May 3, 2022
Accepted: July 22, 2022
Published: August 5, 2022

https://doi.org/10.1021/acsomega.2c02501
ACS Omega 2022, 7, 28275−28283

output enhancement by metal electrode corrosion. We further show that the WEIG configuration creates different potentials and chemical environments for the top and bottom electrodes. These differences work synergistically to facilitate electrode corrosion. While such Galvanic WEIGs utilizing only one electrolyte solution are compact and easy to fabricate, they do eventually consume the metal electrodes. They are green nonetheless because Cu, St, and Al are widely available as waste materials, and sea water is plentiful. The simple fabrication of Galvanic WEIGs may provide an incentive for the recycling of waste metals.

EXPERIMENTAL SECTION

Materials. Polyacrylonitrile (PAN) with a number-average molecular weight of 150 kDa was purchased from Sigma-Aldrich. *N*,*N*-Dimethylformamide (DMF) was purchased from EMD Millipore Corporation. Adhesive copper foil tape, 6.0 mm wide and 0.45 mm thick, used as electrodes was produced by Peyou and purchased from Amazon. The colloidal graphite ink was purchased from Electron Microscopy Sciences. Cold-rolled steel sheet, 0.79 mm thick, was purchased from the home renovation store Rona. Aluminum electrodes were prepared from commercial 0.25 mm-thick premium quality aluminum foil (ALCAN) produced by Reynolds Consumer Products Canada Inc. The fiberglass mesh (produced by Pazaka), used as the support for CNMs in one case, was purchased from Amazon and features square holes of the side length of 2.0 mm and a pore density of 224 holes per square inch.

Material Characterization Facilities. The morphologies of the nanofiber mats were analyzed using a Thermo Fisher Quanta 250 eSEM. For composition analysis, an EDAX Element energy dispersive spectrometer (EDS) detector was used.

Electrospun Nanofiber Mats. To prepare electrospun nanofiber mats, PAN was stirred in 90 °C DMF at 300 rpm for 3 h to yield an 8.0 wt % homogeneous solution. After cooling, 12.0 mL of this solution was drawn into a syringe bearing a 22 G needle with a bore diameter of 0.7 mm before the syringe was mounted onto a pump. Electrospinning was performed using a voltage drop of 18.0 kV and a distance of 20.0 cm between the tip of the syringe needle and a 12.0 cm × 12.0 cm glass plate collector that bore an aluminum foil on its back side. The solution pumping rate was 0.397 mL/h, and the total fiber collection time was 24 h per mat. Each spun mat was dried overnight in an oven at 100 °C before it was cooled, detached from the collector, and cut with scissors into the targeted dimension of 2.0 × 4.0 cm^2.

Carbonization. To carbonize the PAN nanofibers, a mat was sandwiched between two quartz plates, each with a mass of 7.4 g and an area of 3.5 × 6.0 cm. The mat was then heated in air under the weight of one quartz plate to 280 °C at 2 °C/min and held at the final temperature for 1 h to stabilize PAN. Subsequently, the furnace atmosphere was replaced with N_2, and a mat was heated to a final temperature of 900 °C at 3 °C/min and held at the final temperature for 60 min.

Plasma Treatment. Plasma treatment of each CNM was performed in a Tergeo plasma cleaner (Pie Scientific) at 35 W and an oxygen flow rate of 30 standard cubic centimeters per minute. The treatment time for each sample was 1 min.

WEIG Fabrication. To fabricate a WEIG, a CNM was placed on a microscopic slide or, in one case, on a fiberglass mesh. The slides were cleaned via sonication in a mixture of acetone, ethanol, and water at v/v/v = 2/1/1 for 30 min and dried in an 80 °C oven for 1 h prior to use. After CNM deposition onto the substrate, a 6 mm-wide copper adhesive foil tape was affixed to the top end of the CNM and was used as the top electrode. To the bottom end of the CNM was first attached an electrical insulating tape that was 170 μm thick, 40 mm long, and 9 mm wide to cover the width of the CNM. An adhesive copper foil tape was then bonded over the insulating tape as the bottom electrode. A similar fabrication procedure was used to prepare aluminum (Al) and steel (St) electrodes.

A graphite bottom electrode was obtained by painting the graphite ink onto the preapplied insulating tape and then allowing the solvent to evaporate. Such a C strip was 70 ± 5 μm thick and ∼7 mm wide. To fabricate a top electrode, the graphite ink was directly painted onto the CNM close to the top edge and the supporting glass slide. After solvent evaporation, a bridging C strip that was ∼5 mm wide on the CNM and ∼2 mm wide on the glass substrate was obtained.

WEIG Characterization. The WEIG performance was evaluated at 24 °C and a relative humidity between 30 and 40%. A multi Autolab potentiostat (Metrohm) controlled by Nova electrochemical data acquisition software was used to determine the open-circuit voltage V_o, short-circuit current I_s, and current−voltage (I−V) curves.

To start the characterization, a WEIG was inserted into an empty 100 mL beaker. After the bottom and top electrodes were connected to the "working electrode" and the "counter electrode" ports of the potentiostat, 25 mL of Milli-Q water or a NaCl Solution at 0.0010, 0.0100, 0.100, or 1.00 M was added to the beaker until it was 5 mm above the bottom electrode. The electrochemical measurements were initiated once the solution touched the CNM.

The first characterization involved the determination of a WEIG's open circuit voltage (V_o) using the open circuit potential function of the potentiostat. In this mode, the voltage produced by the WEIG was measured as a function of time, while the current flow through the external circuit was kept at zero. The measurement was stopped once a stable voltage was achieved, which normally occurred within 30−60 min.

Next, the I−V curves were obtained by using the cyclic voltammetry (CV) function of the potentiostat. Depending on the electrode type, the voltage was scanned somewhere in the range between −1.2 and +0.6 V at a sweeping rate of 100 mV/s. I_s was obtained from the average of the two intercepts made by each CV curve to the current axis that crosses the voltage axis at zero.

To determine how the V_o and I_s values of C/C, C/Cu, and Cu/Cu WEIGs changed with the time of their operation in a 0.100 M NaCl solution, cells after the determination of their initial V_o and I_s values were short-circuited by connecting their top and bottom electrodes with Cu wires. To remeasure the V_o and I_s values at a given operation time, the electrodes were disconnected and connected to the working and counter electrode ports of the potentiostat. The procedure mentioned above for V_o and I_s measurement of pristine WEIGs was utilized to determine V_o and I_s WEIGs that were operating between 0 and 120 h.

Potentials of Individual Electrodes. To measure individually the potentials of the top and bottom electrodes of different WEIGs, the standard three-electrode configuration was used. While the electrode of interest was used as the "working electrode," the other electrode of the WEIG was used as the "counter electrode." The "reference electrode" was an

https://doi.org/10.1021/acsomega.2c02501
ACS Omega 2022, 7, 28275−28283

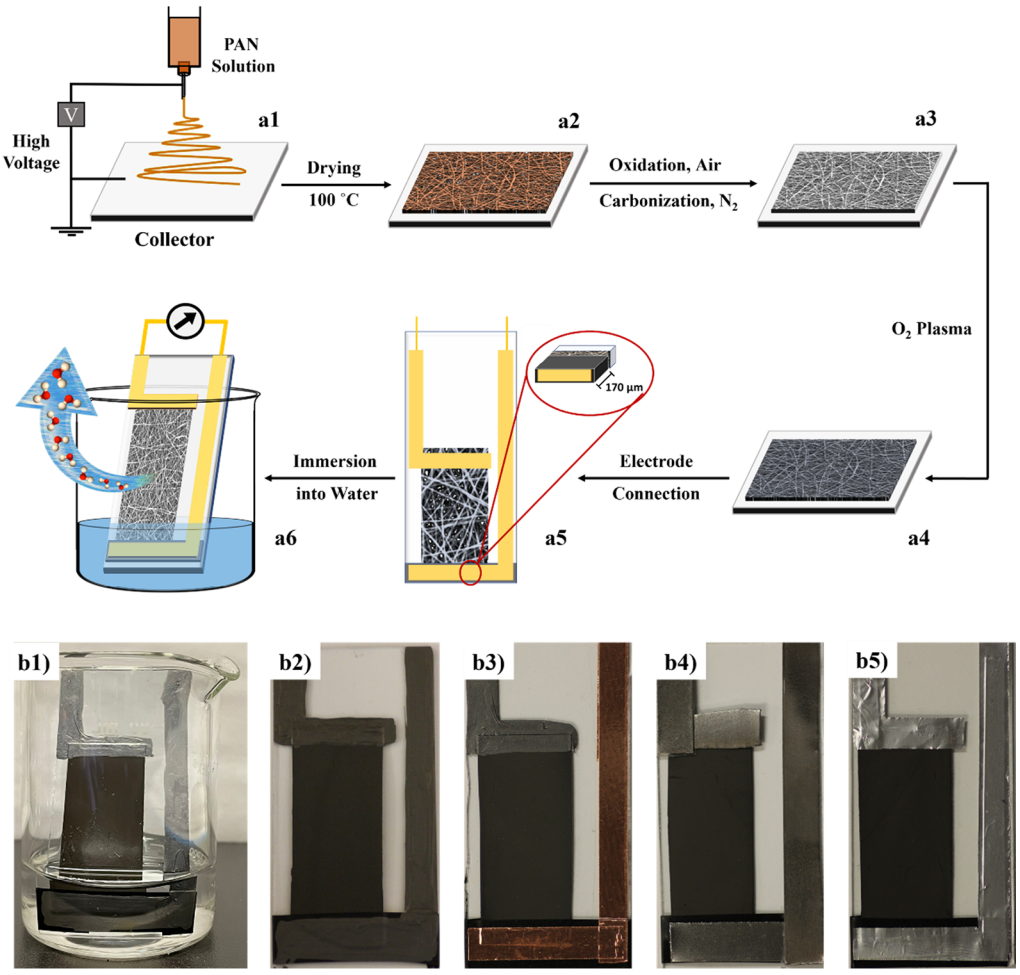

Figure 1. (a) Steps involved for WEIG fabrication, and (b) photographs of (1) a C/C WEIG in 0.100 M NaCl and the core parts of (2) C/C, (3) C/Cu, (4) St/St, and (5) Al/Al WEIGs.

Ag/AgCl/KCl (3 M) electrode that has a potential of 210 mV against the standard hydrogen electrode (SHE). The reference electrode was connected to the operation medium (water or 0.100 M NaCl solution) of a WEIG using a salt bridge made of a U-shaped glass tube filled with Agar swollen with 1 M KNO_3. In a measurement, one end of the salt bridge was placed into the WEIG operation medium about 1−2 mm away from the bottom electrode, which was separated from the conductive CNM by an insulating tape. The measured values were corrected so that the reported E_{top} and E_{bot} values were the potentials of the top and bottom electrodes relative to that of the SHE.

Compact Galvanic WEIGs. A compact Al/Al Galvanic WEIG was fabricated by placing the core part of this WEIG in a plastic box that was 5.1 cm tall, 2.5 cm wide, and 1.1 cm thick rather than a 100 mL beaker. When the lid was open after the addition of 1.0 mL of a 0.100 M NaCl solution, the resultant WEIG displayed the I_s and V_o values of 0.91 V and 1.47 mA. After four of such compact Al/Al Galvanic WEIGs were connected in series, a voltage of 3.76 V and a current of 1.47 mA were measured for the WEIG pack using a normal multimeter.

RESULTS AND DISCUSSION

WEIG Fabrication. The hydrophilic CNMs were prepared in several steps.[17] First, a PAN solution was electrospun to yield a PAN nanofiber mat (Figure 1a1). After drying at 100 °C (a1 → a2), the mat was heated in air at 280 °C for 1 h to convert PAN into ladder-like moieties and then heated under nitrogen at 900 °C for 1 h for carbonization (a2 → a3). The mat was hydrophilized by treatment with oxygen plasma for 1 min (a3 → a4). The carbon nanofibers possessed a diameter of 162 ± 24 nm. The mats were 110 ± 5 μm thick, 2.0 cm wide, and 4.0 cm long.

To construct a WEIG, a CNM was first placed on a microscope glass slide before an insulating adhesive tape (9 mm wide, 40 mm long, and 170 μm thick) was placed across the width at the bottom end of the CNM. The insulating tape was used mainly to avoid a short circuit but to allow the probing of the streaming potential generated in the aqueous phase in the nanochannels of a WEIG. Subsequently, a carbon strip (obtained by evaporating water from a graphite ink), a Cu or Al foil, or a steel strip was applied onto this insulating tape to form the bottom electrode, while the top electrode was applied directly onto the CNM without using a spacing insulating tape (a4 → a5). After the two electrodes were connected with copper wires to an external circuit and the assembly was placed into a 100 mL beaker, 25 mL of Milli-Q water or a NaCl solution was added to submerge the bottom electrode and to start the operation of the WEIG. While Figure 1a6 shows a schematic of a Cu/Cu WEIG and Figure 1b1 shows a photograph of a C/C WEIG, Figure 1b2−b5 shows

https://doi.org/10.1021/acsomega.2c02501
ACS Omega 2022, 7, 28275−28283

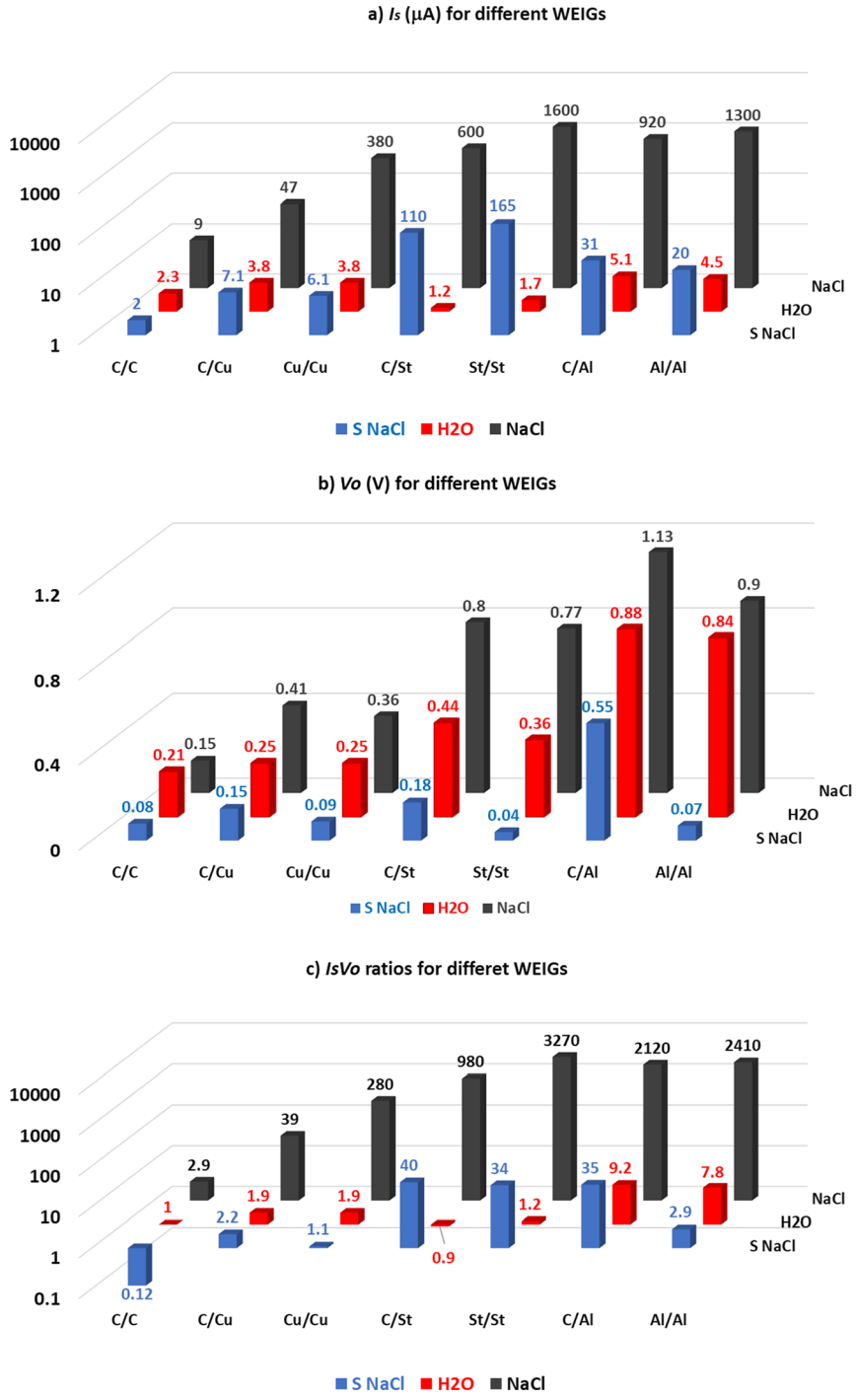

Figure 2. Plots of (a) I_s and (b) V_o values for normal WEIGs operating in Milli-Q water (H_2O) and 0.100 M NaCl (NaCl), as well as for WEIGs submerged under 0.100 M NaCl (S NaCl). Plot (c) shows how the ratio between the I_sV_o value of a given WEIG and that of the C/C WEIG operating in water changes with the WEIG type and operation medium.

photographs of the core parts of C/C, C/Cu, St/St, and Al/Al WEIGs.

Electric Characteristics of the WEIGs. The "open circuit potential" program of a potentiostat was used to determine the open-circuit voltage, V_o. This was followed by starting the CV program to obtain CV curves at a scanning rate of 100 mV/s. While the CV curves from the first five scans for all WEIGs operating in different media are shown in Figures S3, Figures S1e–h show the CV curves from the second scan for the C/C, C/Cu, C/steel, and C/Al WEIGs operating in Milli-Q water. The I_s value for each WEIG was obtained from the average of the two intercepts made by each CV curve from the second scan to the current axis. Table S1 in the Supporting Information lists the I_s and V_o values thus determined for the different WEIGs operating in either water or 0.100 M NaCl solution, and each value represents the average of three separate WEIGs of a given type plus its standard deviation. These results are replotted in Figure 2, while the corresponding errors that are provided in Table S1 are omitted for aesthetic appeal and clarity.

https://doi.org/10.1021/acsomega.2c02501
ACS Omega 2022, 7, 28275−28283

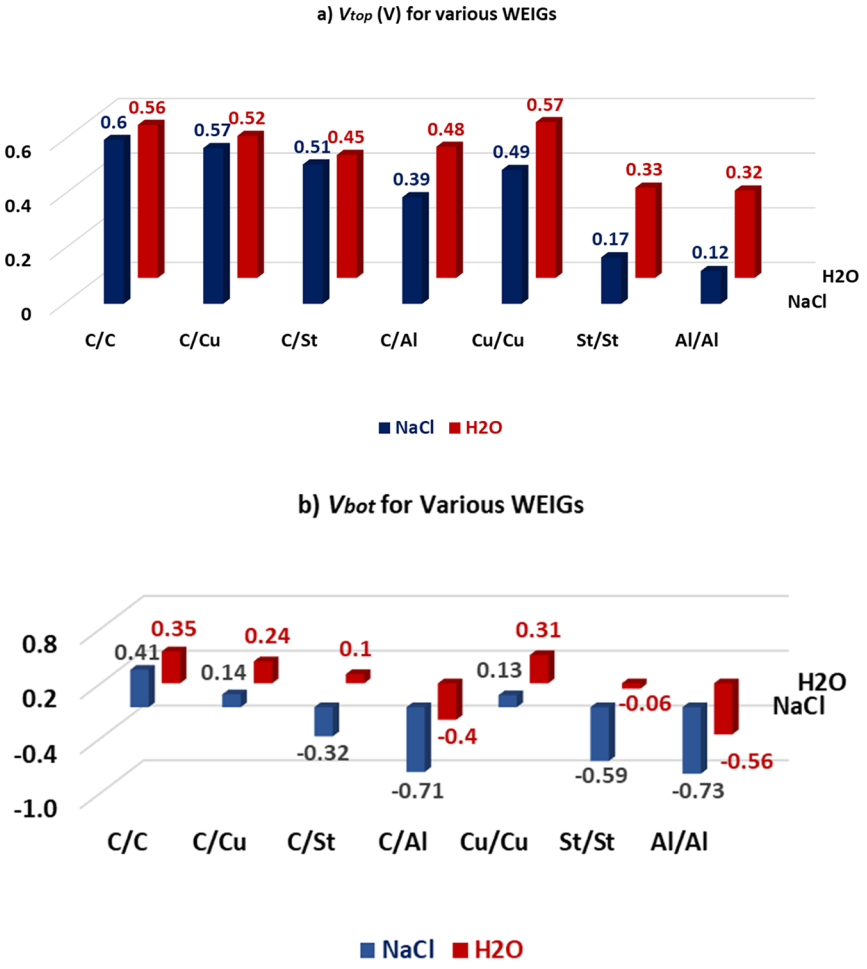

Figure 3. Plots of the electric potentials, E_{top} and E_{bot}, of the (a) top and (b) bottom electrodes, respectively, relative to that of the SHE for various WEIGs operating in different media.

Figure 2c also shows how the ratio between the I_sV_o value of a given WEIG and that of the C/C WEIG operating in water changes with the WEIG type and operation medium. The different I_sV_o values are compared because the current I through an external circuit driven by an ideal WEIG increases linearly with the potential drop V across the circuit, and the maximum power output of such a WEIG is $I_sV_o/4$.

WEIGs Operating in Milli-Q Water. The average I_s and V_o values of three C/C WEIGs are 2.3 ± 0.1 and 0.21 ± 0.02 V (Table S1 and Figure 2a,b), respectively. Owing to the inertness and similarity of the two electrodes, which are comprised of a bottom graphite electrode (strip) and a composite "top" electrode consisting of a conducting CNM infused with a top graphite strip, the current and potential measured in this case should be mostly due to the electrokinetic effect. We verified this assumption by comparing the I_sV_o values of a C/C WEIG in water before and 15 min after its CNM was wrapped with a parafilm film. The wrapping impeded the evaporation and thus slowed the rising of water in the CNM, causing the WEIG's I_sV_o to drop by 93%. We also added enough water to completely submerge the top electrode to yield a "submerged WEIG" featuring no capillary water rise. The submersion decreased the I_s and V_o values from 2.3 ± 0.1 μA and 0.21 ± 0.02 V to 0.5 ± 0.2 μA and 0.05 ± 0.01 V, respectively, corresponding to a I_sV_o drop of 95 ± 2%. Since the $I-V$ curves of these WEIGs are straight lines, and the maximum power output of these devices is $I_sV_0/4$, the >90% drop in I_sV_o when water rising was eliminated suggests that the electrokinetic effect accounted for >90% of the measured power output for the C/C WEIGs operating in water.

The I_s and V_o values did not reach zero even for the wrapped and submerged WEIGs because the top and bottom electrodes are similar but are still compositionally different. Additionally, the positive signs of the measured I_s and V_o values suggest that the cations such as protons rose in the pores of the CNMs. The dissociation of cations from the fibers is possible because the zeta potential of fragments of these fibers was negative in water.[17]

When the bottom electrode is changed from Cu to St and then to Al, the V_o value of the C/metal or the metal/metal WEIGs operating in water increases due to the decrease in the oxide reduction potential of the metals. Despite the higher V_o, I_s of the metal-containing WEIGs is increased by less than 2.5-fold relative to that of the C/C WEIG. This result suggests that the surfaces of these metal electrodes were passivated by compact and dense oxide layers that were not readily perforated in water.[26,27] These oxide layers blocked access of the bottom metal electrodes by OH^- or water and impeded the oxidation of the metal electrodes in Milli-Q water. Based on the low ratios of the I_sV_o values of the C/Cu, Cu/Cu, C/St, and St/St WEIGs relative to that of the C/C WEIG, the power outputs of these WEIGs should be mostly derived from the electrokinetic effect.

https://doi.org/10.1021/acsomega.2c02501
ACS Omega 2022, 7, 28275−28283

In the previous paragraphs, we have intentionally avoided the quantification of contributions made by the electrokinetic effect and redox reactions to the measured V_o and I_s values because this is a challenging task. As will be discussed later, the electrokinetic effect and redox reactions work synergistically to boost each other in a Galvanic WEIG, and the power produced when these two effects operate in unison is much greater than the sum of powers produced from each effect operating alone. Thus, we cannot assume that V_o or I_s is the sum of voltages or currents produced from the electrokinetic effect and a redox reaction operating alone. If we have to quantify the percentage ϵ of contributions made by redox reactions toward the power output of a metal-bearing WEIG, eq 1 can be used

$$\in = \frac{(I_sV_o)_m - (I_sV_o)_c}{(I_sV_o)_m} \times 100\% \quad (1)$$

where $(I_sV_o)_m$ and $(I_sV_o)_c$ are the I_sV_o values for a metal-bearing WEIG and a C/C WEIG, respectively. Using eq 1, the ϵ values for the C/Cu, C/St, C/Al, Cu/Cu, St/St, and Al/Al WEIGs operating in water are 48 ± 25, 0, 89 ± 26, 48 ± 8, 18 ± 14, and 87 ± 19%, respectively.

WEIGs Operating in NaCl Solutions. In a 0.100 M NaCl solution, the V_o value of the C/C WEIGs decreased somewhat (Figure 2b), and the I_s value increased slightly (Figure 2a), increasing I_sV_o by 2.9 times relative to that measured in water (Figure 2c). A drop in V_o following the replacement of water by a salt solution as the operating medium for a WEIG has been observed by others[6,9] and is caused here by decreases in the zeta potential of the electric double layer around the carbon nanofibers. The higher I_s is attributable to increased contributions from redox reactions of the two nonidentical C electrodes. As the salt concentration increased, the electric resistance between the bottom C electrode and the "top" electrode decreased. The increased ion transport accelerated the redox reactions, such as the reduction of epoxide groups on the surfaces of the carbon fibers and the oxidation of −C═C− units at the bottom C electrode,[28] increasing the redox current.

The V_o values of the metal-containing WEIGs increased substantially (Figure 2b), and I_s increased by up to 1000-fold (Figure 2a) when the operation medium was changed from water to 0.100 M NaCl or other NaCl solutions (Figure S3). For the C/Cu, C/St, and C/Al WEIGs in 0.100 M NaCl, their I_sV_o values increased by 39, 980, and 2120 times, respectively. Meanwhile, the I_sV_o enhancement factors were 280, 3270, and 2410 for the Cu/Cu, St/St, and Al/Al WEIGs.

The I_s value increased drastically in a NaCl solution because the metal oxide layers on the electrodes were perforated or destroyed by Cl^- ions. In the case of Cu, the reaction:

$$Cu_2O + 2H^+ + 2Cl^- \rightleftharpoons 2CuCl + H_2O \quad (2)$$

converts a compact passivating Cu_2O layer into a loose CuCl layer.[26,27] At sufficiently high NaCl concentrations, CuCl can even be converted into the soluble $CuCl_2^-$.[26,27] Exposure to OH^- facilitates Cu oxidation to Cu_2O via the following reaction, for example

$$2Cu(s) + 2OH^- \rightleftharpoons Cu_2O(s) + H_2O + 2e^- \quad (3)$$

To gain insights into the V_o changes, we determined the electric potentials, E_{top} and E_{bot}, of the top and bottom electrodes of various WEIGs, respectively, relative to that of the standard hydrogen electrode (SHE). The results are summarized in Table S2 and Figure 3.

Results of Figure 3 reveal several trends. First, E_{top} changes only slightly especially among the C/metal WEIGs. Second, E_{bot} decreases from Cu to St and then further to Al for either the C/metal or the metal/metal WEIG series in either water or 0.100 M NaCl. Third, changing the operation medium from Milli-Q water to 0.100 M NaCl caused a substantial drop in E_{bot} for a given WEIG. Since $V_o = E_{top} - E_{bot}$, the changes in E_{bot} were mainly responsible for the observed V_o variations among the different WEIGs.

E_{bot} changes from metal to metal because their oxidation potentials differ. Equations S1−S3 (Supporting Information) provide possible oxidation reactions of Cu, Fe, and Al and their associated oxidation potentials. Moving from Cu to Fe and then to Al, the reduction potentials of their oxides decrease following the decreasing trend in E_{bot}.

E_{bot} for a metal-bearing WEIG drops as the operating medium is changed from water to a NaCl solution due to the increased accessibility of the electrode. For a Cu bottom electrode undergoing reaction 2, its Nernst equation is

$$E_{bot} = -0.36 - 0.059 \log_{10}[OH^-]\ V \quad (4)$$

As the metal surfaces became accessible and the probed OH^- concentration increased, E_{bot} decreased.

The reduction reaction involving metal corrosion is normally[29,30]

$$(1/2)O_2 + H_2O + 2e^- \rightleftharpoons 2OH^- \quad (5)$$

with its reduction potential given by

$$E = 0.401 + 0.059\text{pOH} + 0.148 \times \log_{10}P_{O_2}\ V \quad (6)$$

Since the major reaction at the top electrode is the same regardless of the electrode used, E_{top} should not change significantly from one electrode to another, as is observed here. We further note that this reaction is indeed possible because the measured E_{top} values are ∼0.5 V. This value can be achieved from eq 6 by assuming the appropriate O_2 pressure P_{O2} and OH^- concentrations at the top electrode, which is a composite electrode, as discussed in the Supporting Information.

We performed various experiments to seek support for the proposed redox reactions. To demonstrate the involvement of O_2, we determined the I_s and V_o values of three C/Al WEIGs operating in 0.100 M NaCl in an inflatable polyethylene glove bag that was briefly evacuated and then backfilled with N_2 or O_2. These values were 86 ± 9 μA and 0.89 ± 0.02 V, respectively, under N_2 and increased to 487 ± 27 μA and 1.02 ± 0.05 V when the atmosphere was changed to O_2. The I_s value did not decrease to zero even under N_2 because O_2 could not have been fully removed from such a bag under our experimental conditions.

As discussed in the Supporting Information, energy dispersive spectroscopy (EDS) and other methods were used to identify the oxidized products formed on the bottom electrodes of metal-bearing WEIGs. For the C/Cu and Cu/Cu WEIGs, the major oxidized product was Cu_2O. Meanwhile, it was most likely that a mixture of $Fe(OH)_2$, Fe_2O_3, and $Fe(OH)_3$ at the bottom electrode of the C/St or St/St WEIGs (Figure S6). For the C/Al and Al/Al WEIGs, Al^{3+} was the major product. Titration of the used salt solution with 1.0 M NaOH produced a precipitate, which was indicative of $Al(OH)_3$ or Al_2O_3 formation. This precipitate redissolved

https://doi.org/10.1021/acsomega.2c02501
ACS Omega 2022, 7, 28275−28283

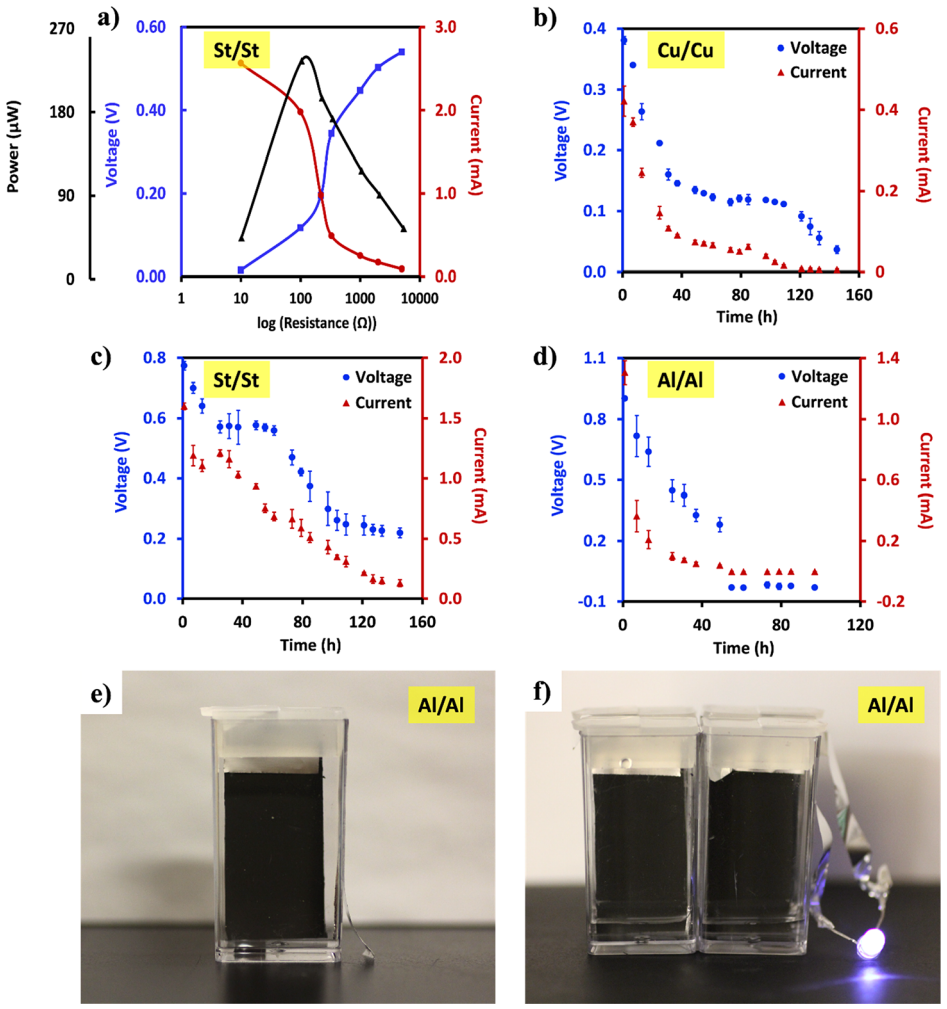

Figure 4. (a) Variation in I_{ex}, V_{ex}, and output power $I_{ex}V_{ex}$ as a function of external (ex) load R_{ex} for a St/St WEIG operating in 1.00 M NaCl. The plotted values are the averages for three WEIGs, and the error bars are not shown to allow a clear viewing of the different sets of data. Also shown are variations in the I_s and V_o values of (b) Cu/Cu, (c) St/St, and (d) Al/Al WEIGs operating in 0.100 M NaCl solution as a function of the cell operation time under short-circuit conditions, as well as photographs of € a compact Al/Al WEIG, and (f) four such WEIGS being used to illuminate a white-light LED.

upon further titration with a 10 M NaOH solution that was indicative of $Al(OH)_4^-$ formation.[29]

Another trend revealed by Figure 2b is that the I_s value was further increased from a C/metal WEIG to its corresponding metal/metal WEIG operating in a NaCl solution. In a C/metal WEIG, the OH^- ions produced from the reduction of oxygen at the "top electrode" diffuse to the bottom electrode to become consumed. In a metal/metal WEIG, the OH^- ions produced near the top metal electrode can be partially consumed via a side reaction. For a Cu top electrode, for example, the side reaction can be

$$Cu + 2OH^- + (1/2)O_2 \rightleftharpoons CuO + H_2O \quad (7)$$

We have deduced CuO formation at the top electrode again via EDS analysis or from the green color of the formed product (Figure S2j). Although this reaction, unlike Galvanic corrosion, does not produce electrons that flow through the external circuit, the elimination of some OH^- ions near the electrode can reduce the polarization potential derived from an electric double layer formed at the electrode/solution interface. The partial elimination of this electrode polarization effect increased the I_s value for the main corrosion reactions occurring at the different electrodes.[31]

Galvanic WEIGs. Galvanic cells normally consist of compositionally different metal electrodes immersed in separate solutions that are connected by a salt bridge or separated by a porous membrane.[31] The metal/metal WEIGs here operate despite the use of the same metal as the top and bottom electrodes and the use of a single electrolyte solution. Such a Cu/Cu, St/St, or Al/Al WEIG produces electricity because the two electrodes are at different potentials due to a streaming potential and their different chemical environments. These differences cause the bottom electrode to become cathodic and the top metal electrode anodic despite their intrinsically identical chemical compositions. The use of a single electrolyte solution simplifies Galvanic cell fabrication.

The role played by the environmental asymmetry and the potential difference between the two electrodes of a meta/metal WEIG operating in 0.100 M NaCl is best witnessed by comparing the I_sV_o values of a normal and a submerged WEIG. The I_sV_o values of submerged Cu/Cu, St/St, and Al/Al WEIGs are decreased by 99.6, 99.5, and 99.9%, respectively, relative to their Galvanic counterparts (Figure 2c). Therefore, the

https://doi.org/10.1021/acsomega.2c02501
ACS Omega 2022, 7, 28275−28283

Galvanic reactions empower a metal-containing WEIG, and the WEIG configuration works synergistically, in turn, to facilitate the Galvanic corrosion of the metal electrodes.

Power Output, Service Life, and Compact Galvanic WEIGs. To gain a better view of the power characteristics of the metal/metal WEIGs, we performed loading studies of St/St WEIGs prepared on a fiberglass mesh operating in 1.00 M NaCl and Milli-Q water. The porous substrate was used rather than a glass slide to accelerate water evaporation,[17] and a higher than normal NaCl concentration was utilized to increase the output of such a WEIG (Figure S4). Figures 4a and S7 show the results of the loading studies. The maximum power outputs from such devices (3 in each case) operating in the 1.00 M NaCl solution and water are 232 ± 33 μW and 165 ± 19 nW at external resistance loadings of 100 Ω and 100 kΩ, respectively. Since the area of the CNM is 8.0 cm^2, the respective areal power densities of this device are 29 ± 5 $\mu W/cm^2$ and 21 ± 3 nW/cm^2 in the two media. Thus, the use of NaCl increased the output density of the St/St WEIG by (1.4 ± 0.3) × 10^3 times.

One may have the urge to use the power outputs for the above two types of WEIGs and an equation similar to eq 1 to quantify the contributions that are made by the electrokinetic effect and redox reactions to the power output of a Galvanic WEIG. However, we caution against such an attempt because the electrokinetic effect and redox reactions work synergistically to boost each other in a Galvanic WEIG, and the power produced when these two effects operate in unison is much greater than the sum of powers produced from each effect operating alone. For example, the power output of a WEIG operating 0.100 M NaCl without the electrokinetic effect may be reduced by up to 99.9%, as discussed above.

Figure 4b–d shows how the I_s and V_o values of the Cu/Cu, St/St, and Al/Al WEIGs changed with operation time in a 0.100 M NaCl solution under short-circuit conditions, which were used to maximize current dissipation. The lifetime decreased from the St/St to the Cu/Cu and Al/Al WEIG, following the decreasing trend in the electrode thickness (Supporting Information).

The need for only one electrolyte solution prompted us to fabricate a compact Al/Al WEIG in a rectangular plastic container that is 5.1 cm tall, 2.5 cm wide, and 1.1 cm thick (Figure 4e). This WEIG can be capped and portable. When four such compact WEIGs were connected in series, the WEIG pack gave a current reading of 1.47 mA and a voltage of 3.76 V, as measured using a normal multimeter. Figure 4f shows that the pack can light a LED bulb, and this bright illumination was maintained continuously for ∼80 h before the light intensity was seen visually to dim and disappear eventually by 106 h.

We want to point out finally that the output of a WEIG cell can be further increased by increasing the width of the CNM. We have shown previously that the I_s value of WEIG cells increased linearly with the width of the CNM.[17]

CONCLUSIONS

In summary, various electrodes have been used for the fabrication of CNM-based WEIGs. Our systematic study indicates that the C/C, C/Cu, Cu/Cu, C/St, Cu/Cu, and St/St WEIGs in water harnessed mostly the streaming currents and potentials. The replacement of water with a NaCl solution as the operation medium activates Galvanic corrosion of the bottom metal electrodes and drastically increases the power output of the devices. A Galvanic St/St WEIG operating in 1.00 M NaCl has a high output density of 29 $\mu W/cm^2$. This output drops by 99.9% when the streaming potential and asymmetric environments of the two electrodes are eliminated by submerging both electrodes into the salt solution. Thus, the WEIG configuration facilitates Galvanic corrosion, and Galvanic corrosion empowers WEIGs. While the high electric output and the simplicity of assembling these Galvanic WEIGs facilitate their practical applications and provide an incentive for metal recycling, one should cautiously choose one's electrodes if one's intention is to fabricate a WEIG. Last but not the least, we are the first to determine the electric potentials of the individual electrodes relative to that of the SHE. Such information provides insights into the redox reactions occurring in a WEIG and should be used regularly in the future for WEIG characterization..

ASSOCIATED CONTENT

Supporting Information

The Supporting Information is available free of charge at https://pubs.acs.org/doi/10.1021/acsomega.2c02501.

Photographs and CV curves of WEIGs, SEM image of a corroded Cu electrode from a C/Cu WEIG, loading curve of a St/St WEIG operating in water, as well as discussion of nonzero I_s and V_o values of the submerged C/C WEIGs, effect of varying NaCl concentration, electric potentials of top and bottom electrodes, possible oxidation reactions, and products at the bottom metal electrodes (PDF)

AUTHOR INFORMATION

Corresponding Author

Guojun Liu − *Department of Chemistry, Queen's University, Kingston, Ontario K7L 3N6, Canada;* orcid.org/0000-0002-9643-5070; Email: gliu@chem.queensu.ca

Authors

Tina Tabrizizadeh − *Department of Chemistry, Queen's University, Kingston, Ontario K7L 3N6, Canada*

Zhe She − *Department of Chemistry, Queen's University, Kingston, Ontario K7L 3N6, Canada*

Kevin Stamplecoskie − *Department of Chemistry, Queen's University, Kingston, Ontario K7L 3N6, Canada;* orcid.org/0000-0002-0232-9956

Complete contact information is available at: https://pubs.acs.org/10.1021/acsomega.2c02501

Notes

The authors declare no competing financial interest.

ACKNOWLEDGMENTS

The New Frontier Research Fund and NSERC Discovery Grant RGPIN/04307-2019 are gratefully acknowledged for sponsoring this research. Jiandong Wang is thanked for performing the SEM and SEM/EDS measurements.

REFERENCES

(1) Lyklema, J. *Fundamentals of Interface and Colloid Science*; Acadmic Press, 1995.

(2) Yang, J.; Lu, F. Z.; Kostiuk, L. W.; Kwok, D. Y. Electrokinetic microchannel battery by means of electrokinetic and microfluidic phenomena. *J. Micromech. Microeng.* **2003**, *13*, 963–970.

(3) Olthuis, W.; Schippers, B.; Eijkel, J.; van den Berg, A. Energy from streaming current and potential. *Sens. Actuators, B* **2005**, *111*−*112*, 385−389.
(4) van der Heyden, F. H. J.; Bonthuis, D. J.; Stein, D.; Meyer, C.; Dekker, C. Electrokinetic energy conversion efficiency in nanofluidic channels. *Nano Lett.* **2006**, *6*, 2232−2237.
(5) van der Heyden, F. H. J.; Bonthuis, D. J.; Stein, D.; Meyer, C.; Dekker, C. Power generation by pressure-driven transport of ions in nanofluidic channels. *Nano Lett.* **2007**, *7*, 1022−1025.
(6) Xue, G. B.; Xu, Y.; Ding, T. P.; Li, J.; Yin, J.; Fei, W. W.; Cao, Y. Z.; Yu, J.; Yuan, L. Y.; Gong, L.; Chen, J.; Deng, S. Z.; Zhou, J.; Guo, W. L. Water-evaporation-induced electricity with nanostructured carbon materials. *Nat. Nanotechnol.* **2017**, *12*, 317−321.
(7) Zhang, Z. H.; Li, X. M.; Yin, J.; Xu, Y.; Fei, W. W.; Xue, M. M.; Wang, Q.; Zhou, J. X.; Guo, W. L. Emerging hydrovoltaic technology. *Nat. Nanotechnol.* **2018**, *13*, 1109−1119.
(8) Li, J.; Liu, K.; Xue, G. B.; Ding, T. P.; Yang, P. H.; Chen, Q.; Shen, Y.; Li, S.; Feng, G.; Shen, A. G.; Xu, M.; Zhou, J. Electricity generation from water droplets via capillary infiltrating. *Nano Energy* **2018**, *48*, 211−216.
(9) Dao, V. D.; Vu, N. H.; Choi, H. S. All day Limnobium laevigatum inspired nanogenerator self-driven via water evaporation. *J. Power Sources* **2020**, *448*, 227388.
(10) Lyu, Q. Q.; Peng, B. L.; Xie, Z. J.; Du, S.; Zhang, L. B.; Zhu, J. T. Moist-Induced Electricity Generation by Electrospun Cellulose Acetate Membranes with Optimized Porous Structures. *ACS Appl. Mater. Interfaces* **2020**, *12*, 57373−57381.
(11) Yun, T. G.; Bae, J.; Rothschild, A.; Kim, I. D. Transpiration Driven Electrokinetic Power Generator. *ACS Nano* **2019**, *13*, 12703−12709.
(12) Li, L. H.; Hao, M. M.; Yang, X. Q.; Sun, F. Q.; Bai, Y. Y.; Ding, H. Y.; Wang, S. Q.; Zhang, T. Sustainable and flexible hydrovoltaic power generator for wearable sensing electronics. *Nano Energy* **2020**, *72*, 104663.
(13) Shao, C. X.; Ji, B. X.; Xu, T.; Gao, J.; Gao, X.; Xiao, Y. K.; Zhao, Y.; Chen, N.; Jiang, L.; Qu, L. T. Large-Scale Production of Flexible, High-Voltage Hydroelectric Films Based on Solid Oxides. *ACS Appl. Mater. Interfaces* **2019**, *11*, 30927−30935.
(14) Wu, M.; Peng, M.; Liang, Z.; Liu, Y.; Zhao, B.; Li, D.; Wang, Y.; Zhang, J.; Sun, Y.; Jiang, L. Printed Honeycomb-Structured Reduced Graphene Oxide Film for Efficient and Continuous Evaporation-Driven Electricity Generation from Salt Solution. *ACS Appl. Mater. Interfaces* **2021**, *13*, 26989−26997.
(15) Li, C.; Yang, D.; Hasan, S. W.; Zhang, X.; Tian, Z. Q.; Shen, P. K. Electricity generation from ionic solution flowing through packed three-dimensional graphene powders. *Nanotechnology* **2021**, *32*, 355401.
(16) Zhang, G.; Duan, Z.; Qi, X.; Xu, Y.; Li, L.; Ma, W.; Zhang, H.; Liu, C.; Yao, W. Harvesting environment energy from water-evaporation over free-standing graphene oxide sponges. *Carbon* **2019**, *148*, 1−8.
(17) Tabrizizadeh, T.; Wang, J.; Kumar, R.; Chaurasia, S.; Stamplecoskie, K.; Liu, G. J. Water-Evaporation-Induced Electric Generator Built from Carbonized Electrospun Polyacrylonitrile Nanofiber Mats. *ACS Appl. Mater. Interfaces* **2021**, *13*, 50900−50910.
(18) Kumar, R.; Tabrizizadeh, T.; Chaurasia, S.; Liu, G. J.; Stamplecoskie, K. Hydrovoltaic power generation from multiwalled carbon nanotubes. *Sustainable Energy Fuels* **2022**, *6*, 1141−1147.
(19) Chaurasia, S.; Kumar, R.; Tabrizizadeh, T.; Liu, G. J.; Stamplecoskie, K. All-Weather-Compatible Hydrovoltaic Cells Based on Al2O3 TLC Plates. *ACS Omega* **2022**, *7*, 2618−2623.
(20) Dao, V. D. An experimental exploration of generating electricity from nature-inspired hierarchical evaporator: The role of electrode materials. *Sci. Total Environ.* **2021**, *759*, 143490.
(21) Qin, Y. S.; Wang, Y. S.; Sun, X. Y.; Li, Y. J.; Xu, H.; Tan, Y. S.; Li, Y.; Song, T.; Sun, B. Q. Constant Electricity Generation in Nanostructured Silicon by Evaporation-Driven Water Flow. *Angew. Chem., Int. Ed.* **2020**, *59*, 10619−10625.
(22) Shao, B. B.; Song, Z. H.; Chen, X.; Wu, Y. F.; Li, Y. J.; Song, C. C.; Yang, F.; Song, T.; Wang, Y. S.; Lee, S. T.; Sun, B. Q. Bioinspired Hierarchical Nanofabric Electrode for Silicon Hydrovoltaic Device with Record Power Output. *ACS Nano* **2021**, *15*, 7472−7481.
(23) Elgrishi, N.; Rountree, K. J.; McCarthy, B. D.; Rountree, E. S.; Eisenhart, T. T.; Dempsey, J. L. A Practical Beginner's Guide to Cyclic Voltammetry. *J. Chem. Educ.* **2018**, *95*, 197−206.
(24) Li, C.; Tian, Z.; Liang, L.; Yin, S.; Shen, P. K. Electricity Generation from Capillary-Driven Ionic Solution Flow in a Three-Dimensional Graphene Membrane. *ACS Appl. Mater. Interfaces* **2019**, *11*, 4922−4929.
(25) Li, Y.; Cui, J.; Shen, H.; Liu, C.; Wu, P.; Qian, Z.; Duan, Y.; Liu, D. Useful spontaneous hygroelectricity from ambient air by ionic wood. *Nano Energy* **2022**, *96*, 107065.
(26) Bianchi, G.; Longhi, P. Copper in sea water, potetnial-pH diagram. *Corros. Sci.* **1973**, *13*, 853−864.
(27) Bjorndahl, W. D.; Nobe, K. Copper corrosion in chloride media - effect of oxygen. *Corrosion* **1984**, *40*, 82−87.
(28) He, S. S.; Zhang, Y. Y.; Qiu, L. B.; Zhang, L. S.; Xie, Y.; Pan, J.; Chen, P. N.; Wang, B. J.; Xu, X. J.; Hu, Y. J.; Dinh, C. T.; De Luna, P.; Banis, M. N.; Wang, Z. Q.; Sham, T. K.; Gong, X. G.; Zhang, B.; Peng, H. S.; Sargent, E. H. Chemical-to-Electricity Carbon: Water Device. *Adv. Mater.* **2018**, *30*, 1707635.
(29) Tejada, S.; Guevara, E.; Olivares, E. Slide projector corrosion cell. *J. Chem. Educ.* **1998**, *75*, 747−748.
(30) Yan, Y.; Timonen, J. V. I.; Grzybowski, B. A. A long-lasting concentration cell based on a magnetic electrolyte. *Nat. Nanotechnol.* **2014**, *9*, 901−906.
(31) Faulkner, L. R.; Bard, A. J.; White, H. S. *Electrochemical Methods: Fundamentals and Applications*, 2nd ed.; Wiley & Sons, 2000.

https://doi.org/10.1021/acsomega.2c02501
ACS Omega 2022, 7, 28275−28283